



Research Article

# Fast and Direct Microwave Synthesis of Carbon from Bovine Blood Waste: A Feedstock Material for Extractive Metallurgy, Carbon Dots Production and Graphite Synthesis

Nikolaos Chalmpes<sup>1</sup>, Georgios Asimakopoulos<sup>1</sup>, Maria Baikousi<sup>1</sup>, Dimitrios Moschovas<sup>1</sup>, Apostolos Avgeropoulos<sup>1</sup>, Athanasios B. Bourlinos<sup>2\*</sup>, Veronika Šedajová<sup>3,4</sup>, Aristides Bakandritsos<sup>5,6</sup>, Dimitrios Gournis<sup>1</sup>, Michael A. Karakassides<sup>1,\*</sup>

<sup>1</sup>Department of Materials Science & Engineering, University of Ioannina, 45110 Ioannina, Greece

<sup>2</sup>Physics Department, University of Ioannina, 45110 Ioannina, Greece

<sup>3</sup>Regional Centre of Advanced Technologies and Materials, Czech Advanced Technology and Research Institute (CATRIN), Palacký University Olomouc, Slezská 27, 77900 Olomouc, Czech Republic

<sup>4</sup>Department of Physical Chemistry, Faculty of Science, Palacký University Olomouc, 17. Listopadu 12, 771 46 Olomouc, Czech Republic

<sup>5</sup>Regional Centre of Advanced Technologies and Materials, Czech Advanced Technology and Research Institute, Palacký University, Křížkovského 511/8, Olomouc 77900, Czech Republic

<sup>6</sup>Nanotechnology Centre, Centre of Energy and Environmental Technologies, VŠB- Technical University of Ostrava 17. Listopadu 2172/15, Ostrava-Poruba 70800, Czech Republic

**\*Corresponding author 1:** Dr. Athanasios B. Bourlinos, Physics Department, University of Ioannina, 45110 Ioannina, Greece.

**\*Corresponding author 2:** Dr. Michael A. Karakassides, Materials Science & Engineering, University of Ioannina, 45110 Ioannina, Greece.

**Received:** 10 October 2021; **Accepted:** 15 October 2021; **Published:** 25 November 2021

**Citation:** Chalmpes N, Asimakopoulos G, Baikousi M, Moschovas D, Avgeropoulos A, Bourlinos AB, Sedajova V, Bakandritsos A, Gournis D, Karakassides MA. Fast and direct microwave synthesis of carbon from bovine blood waste: a feedstock material for extractive metallurgy, carbon dots production and graphite synthesis. Journal of Nanotechnology Research 3 (2021): 011- 028.

## Abstract

Direct irradiation of slaughterhouse bovine blood waste in a domestic microwave oven results in fast carbonization and subsequent formation of carbon nanosheets at yield of 2% after copiously washing off any by-products. Since nearly 5 billion L of slaughterhouse bovine blood is globally produced every year as inevitable part of meat production, the total amount of carbon that could be annually produced by this simple and cost-effective microwave technology reaches the impressive value of 100,000 metric tons per year, albeit the relatively low carbon yield of the process. This large quantity of carbon with well-defined structure and composition could be further exploited in carbothermal extractive metallurgy (e.g., the extraction of copper from copper oxide) or as a cheap and plentiful raw material towards the production of other important carbon materials, such as photoluminescent carbon dots, synthetic graphite and graphene. The direct, simple and affordable microwave conversion of bovine blood waste into useful carbon material represents another example of blood waste valorization that is complementary to the extraction of bioactive compounds for the food or pharmaceuticals industry. It is interesting to note that the same microwave approach can be applied as well for the direct and fast carbonization of expired over the counter medicines, such-like drug effervescent tablets (e.g., analgesic paracetamol), giving carbon at high yield with useful properties (e.g., hexavalent chromium removal).

**Keywords:** Bovine blood; Carbonization; Carbon nanosheets; Microwave heating; Waste management

## 1. Introduction

Blood waste is an inevitable part of the meat industry, which however, due to the high volumes generated from slaughterhouses (e.g., 5 billion L of bovine blood is globally produced every year), it may cause serious pollution problems when directly discarded into the environment as a result of rapid and extensive putrefaction [1]. Hence finding useful applications for blood waste is an important challenge for scientists and meat industry in order to eliminate pollution and prevent loss of potentially valuable material [2,3]. In one example, food industry utilizes about 30 % of the blood waste produced from slaughterhouses as a protein source in food [4]. In another example, the recovery and extraction of bioactive compounds from blood waste has added economic value for pharmaceuticals industry [1]. Lastly, animal blood has served to a less extent as a starting material towards the preparation of functional carbon materials using pyrolytic or hydrothermal methods [5-9]. Nevertheless, no report in the literature refers to the direct microwave conversion of blood waste into carbon. Such a conversion would be of particular interest when considering the large volumes of blood waste produced from slaughterhouses, as well as, the sound benefits of microwave technology.

Microwave synthesis has emerged as a cost-effective, simple and fast preparative technique in materials science, including carbon materials from biomass [10-13]. Besides biomass, animal blood waste could also serve as a cheap and plentiful source of carbon materials under microwaves due to its uniquely complex organic composition (proteins, amino acids, fats, sugars etc.) [14,15]. These organic molecules are excellent carbon precursors upon heating, the latter

potentially induced by microwaves. For instance, blood contains polar molecules in its composition (e.g., water), as well as, dissolved ions (e.g., Na<sup>+</sup>, Cl<sup>-</sup>) that can simultaneously give rise to both dielectric and Ohmic heating upon microwave irradiation [16]. Dielectric heating results from rotation of the polar molecules under the electric field of the electromagnetic radiation, whereas Ohmic heating from ions acceleration and collisions within the medium under the applied electric field. As a result, microwave irradiation of blood is expected to homogeneously raise the temperature high enough in short time to finally induce carbonization of the heat-sensitive biomolecules present in blood. Such a simple, fast and inexpensive microwave approach would allow direct processing of blood waste into carbon in a conventional microwave oven at spot, thus clearly differentiating from time- and energy-consuming pyrolytic methods that require heating at high temperature in resistance ovens.

In the present work we demonstrate the direct and fast microwave conversion of bovine blood waste from a local slaughterhouse into carbon nanosheets. Since blood is a complex mixture of compounds, its microwave treatment resulted as expected in various washable by-products of unknown structure (e.g., deep brown solubles). Therefore, the nanosheets had to be cautiously purified in four steps in order to obtain a carbon product with well-defined structure and composition. Carbon formation was evidenced by X-ray diffraction and Raman spectroscopy, whereas the structural composition and morphology of the nanosheets was verified by X-ray photoelectron spectroscopy and microscopy techniques. Due to the extensive purification steps applied during the process the overall carbon yield

was 2%. However, taking into consideration that nearly 5 billion L of bovine blood waste is produced globally every year in slaughterhouses, it is estimated that about 100,000 metric tons of carbon could be prepared this way. As shown here, this large amount could be further exploited in practical applications, such as extractive metallurgy (e.g., carbothermal extraction of copper metal from copper oxide) or as feedstock material towards the preparation of other valuable nanocarbons (e.g., photoluminescent carbon dots, synthetic graphite and graphene). The present microwave approach is also applicable to medical waste and in particular to expire over the counter drug effervescent tablets (e.g., analgesic paracetamol) towards the high yield production of carbon with useful properties (e.g., in hexavalent chromium removal).

## 2. Materials and methods

30 g bovine blood waste from a local slaughterhouse (Parakalamos Industrial Slaughterhouse, Ioannina, Greece) was placed inside a glass bowl covered on top with a watch glass. The blood was directly irradiated at 700 W for 10 min under rotation using a domestic microwave oven. The produced voluminous carbon mass was collected, crushed into powder and purified in four steps. First, the solid was treated with an HCl aqueous solution at pH = 2 for 24 h followed by washing with water until neutral pH and acetone. Second, the solid was treated with an HF aqueous solution 40 % for another 24 h followed by washing with water until neutral pH and acetone. Third, the solid was copiously washed with N-methyl-2-pyrrolidone (NMP, Aldrich) until no coloration of the solvent was observed, followed by water and acetone washings. Fourth, the solid was finally treated with a saturated EDTA aqueous solution for 1 h under

sonication in an ultrasound bath followed by repeating washings with water and acetone. A black carbon powder was obtained at yield 2 % (N<sub>2</sub> specific surface area: 10 m<sup>2</sup>/g). The yield could be

possibly further improved by either increasing the irradiation time or by using higher microwave power (800 W). The whole process is visualized in Figure 1.



**Figure 1:** Microwave heating of bovine blood waste resulted in a voluminous carbon mass inside the glass bowl. The crude mass was purified as described in the experimental section to afford a fine carbon powder at yield 2 %.

X-ray diffraction (XRD) was conducted on background-free Si wafers using Cu K $\alpha$  radiation from a Bruker Advance D8 diffractometer (Bruker, Billerica, MA, USA). Raman spectra were recorded with a micro-Raman system RM 1000 Renishaw using a laser excitation line at 532 nm. Scanning electron microscopy (SEM) images were obtained using a JEOL JSM-6510 LV SEM Microscope (Ltd., Tokyo, Japan) equipped with an X-Act EDS-detector by Oxford Instruments (Abingdon, Oxfordshire, UK, an acceleration voltage of 20 kV was applied). Atomic force microscopy (AFM) images were collected on silicon wafers in tapping mode with a Bruker Multimode 3D Nanoscope (Ted Pella Inc., Redding, CA, USA). X-Ray Photoelectron Spectroscopy (XPS) measurements were carried out with a PHI VersaProbe II (Physical Electronics) spectrometer using an Al K $\alpha$  source. The obtained spectra were analysed employing the MultiPak (Ulvac-PHI, Ind.) software package. The 284.4 eV peak (carbon C 1s peak) was used as a reference for all binding energies. Photoluminescence spectra were recorded using a luminescence spectrofluorometer

Jasco-8300 (Tokyo, Japan), using a 1 cm path length quartz cuvette. Slit widths with a nominal band pass of 5 nm were used for both excitation and emission ray. The fluorescence emission spectra were recorded from 350 to 650 nm after excitation at different wavelengths.

### 3. Results and Discussion

#### 3.1. Characterization and perspectives of the blood-derived carbon

The XRD pattern of the blood-derived carbon presented in Figure 2, top shows a broad (002) reflection with an interlayer spacing ( $d_{002} = 0.36$  nm) indicative of amorphous carbon composed of stacks of incompletely crystallized layers in turbostratic ordering [17,18]. The sample additionally displays small intensity yet sharp crystalline peaks from a rare form of iron oxide Fe<sub>2</sub>O<sub>3</sub>, namely specularite [19]. This phase apparently aroused from the iron content of the blood (e.g., from the heme group in hemoglobin) and accounted for nearly 0.1 % of the product's composition (i.e., a minute amount), based on thermal quantitative analysis in air. The

amorphous character of the sample was also confirmed by Raman spectroscopy [20] (Figure 2, bottom), showing the typical G and D carbon bands at  $1580\text{ cm}^{-1}$  and  $1377\text{ cm}^{-1}$ , respectively, with a relative intensity ratio of  $\text{ID/IG} = 0.8$  (i.e.,  $> 0.2$  for crystalline graphite [21]). Apart from these features, the sample also exhibits a weak shoulder at  $725\text{ cm}^{-1}$

and a strong yet broad band at  $2846\text{ cm}^{-1}$ , suggestive of nitrogen incorporation from blood proteins and amino acids into the carbon lattice (e.g., nitrogenous carbon) [22]. Lastly, the weak shoulder at  $2228\text{ cm}^{-1}$  is associated with nitrile groups -CN formed in-situ during the carbonization process.

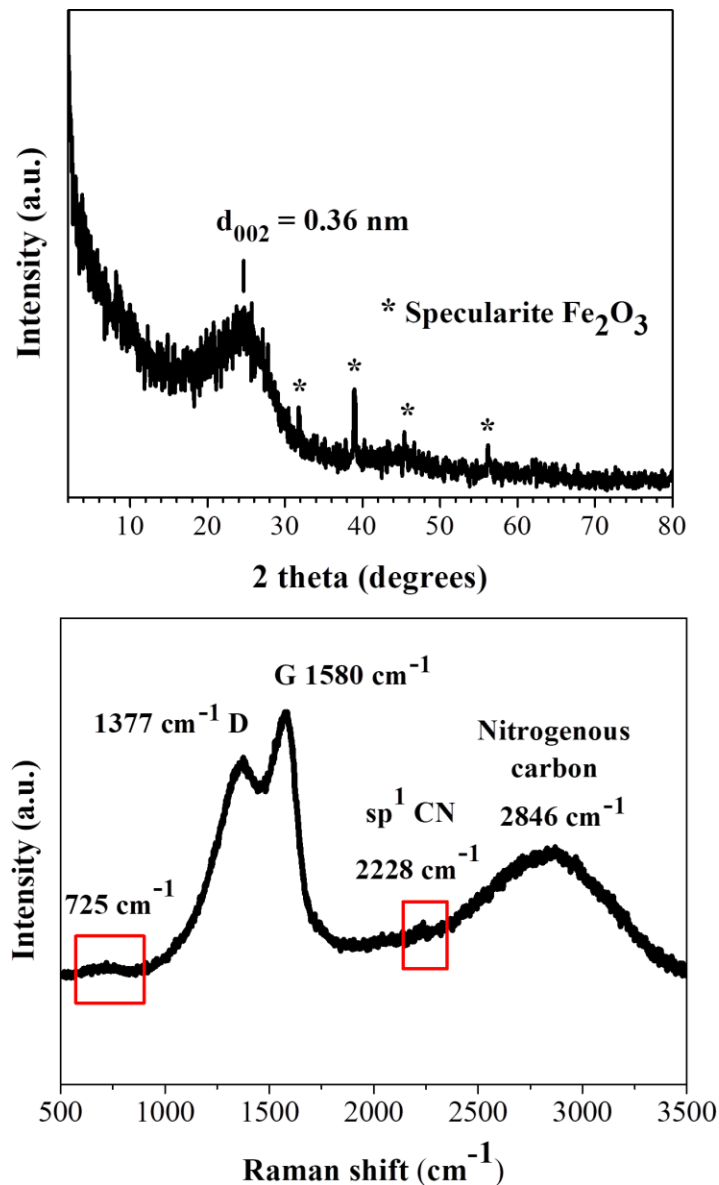


**Figure 2:** XRD pattern (top) and Raman spectrum (bottom) of the blood-derived carbon.

According to SEM study, the blood-derived carbon consists of very large micron-sized plates with multilayer texture near the edges (Figure 3). The

thickness of the platy nanosheets was estimated to be 2.5 nm by AFM (Figure 4).

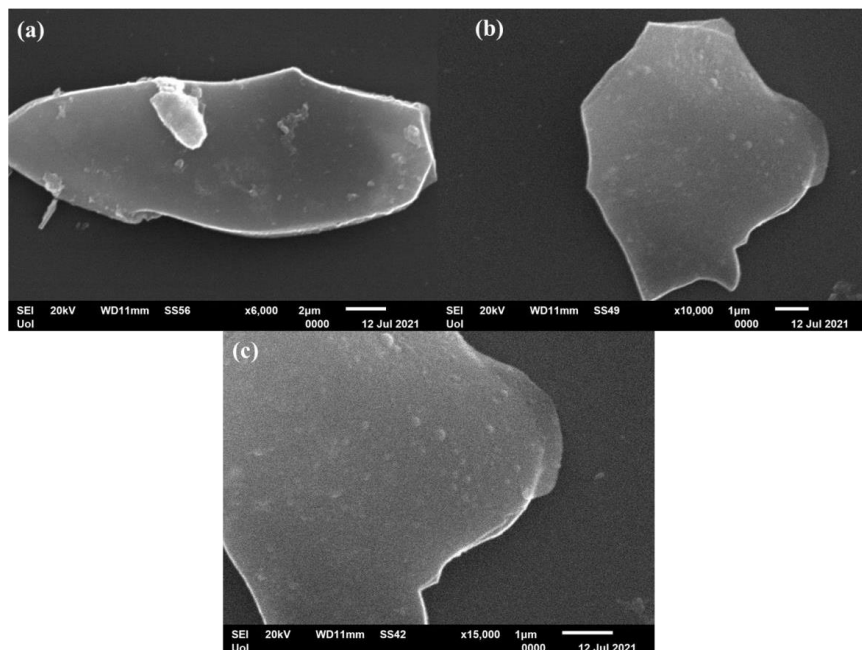


**Figure 3:** SEM portraits of the blood-derived carbon nanosheets.

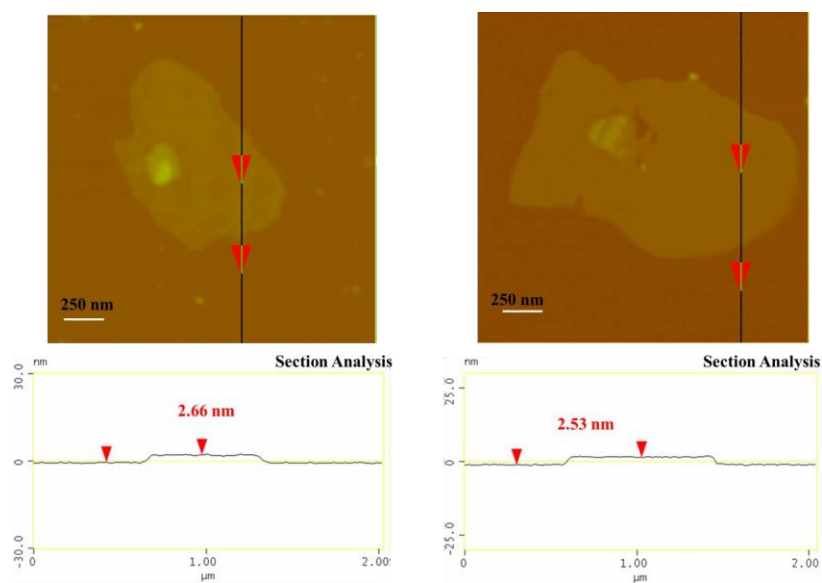


**Figure 4:** AFM images of cross-sectional analysis of selected blood-derived carbon nanosheets with thickness ca. 2.5 nm.

XPS survey analysis reveals the presence of enough carbon (71 %), oxygen (15.5 %), nitrogen (13.3 %) and very little sulphur (0.2 %) in the sample's composition (Figure 5a). No peaks due to Fe were observed in the survey spectrum as a result of minute iron content (< 0.1 %). These elements along with the XRD detectable iron traces originate from the blood's initial composition (e.g., sulfur-containing amino acids, sugars, heme etc.). The deconvolution of the high resolution XPS spectrum of C 1s envelope shows five different components (C=C, C-C, C-O/C-N, C=O and satellite) (Figure 5b). The components

denoted as C=C and C-C are attributed to sp<sup>2</sup> and sp<sup>3</sup> hybridized carbon configurations. The high intensity peak of C-O/C-N bond regions (which are overlapping) [23,24] alongside the peak of C=O bonds confirm the high percentage of both N and O elements in the atomic composition of the sample. Lastly, the N 1s region (Figure 5c) showed three different components, corresponding to pyridinic (44.6 %), pyrrolic (36.7 %) and graphitic (18.7 %) nitrogen bonding states [25]. Note that the deconvolution analysis for sulfur was not possible due to the really small amount of it in the sample.

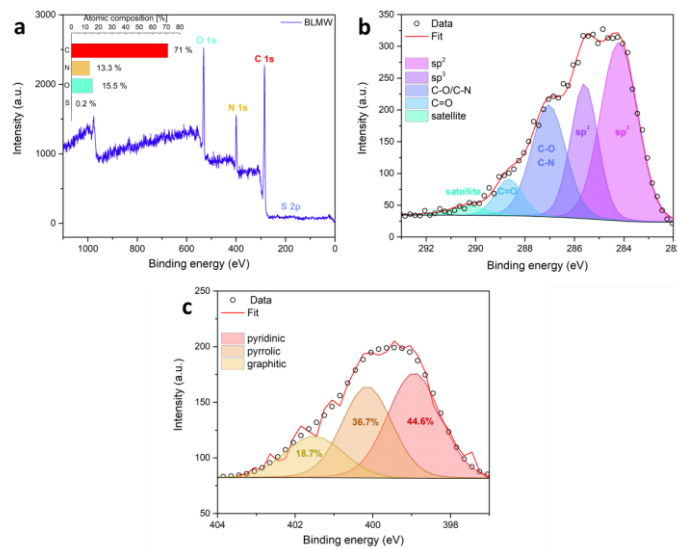


**Figure 5:** a) XPS survey spectrum of the sample with atomic composition (inset). b) Deconvoluted C 1s region with assigned bands. c) The corresponding N 1s region with assigned deconvoluted bands.

On account of its well-defined structure and composition, the blood-derived carbon could be further exploited in important chemical processes, such as in extractive metallurgy for the carbothermal reduction of copper oxide into copper metal, as well as, as plentiful feedstock material for the bottom-down synthesis of photoluminescent carbon dots or the preparation of synthetic graphite by

crystallization of the amorphous carbon nanosheets at high temperature. In the case of carbothermal reduction, a Pyrex glass test tube was charged with 1 g CuO (Fluka, 98 %) and 120 mg of the blood-derived carbon. After the ingredients were mechanically mixed to form a homogeneous black mixture, the test tube was heated until red hot over a gauze flame for few minutes to form metallic copper

inside the tube according to the single displacement reaction  $\text{CuO} + \text{C} \rightarrow \text{Cu} + \text{CO}$  (Figure 6). This process was inspired by the RSC educational experiment of extracting metals with charcoal (see

link: <https://edu.rsc.org/experiments/extracting-metals-with-charcoal/417.article>, last accessed on 8/10/2021).



**Figure 6:** Carbothermal reduction of CuO by the blood-derived carbon. Carbon and CuO were mechanically mixed to give a homogeneous blend (left). The blend was heated until red-hot over a gauze flame for few minutes (middle) to release metallic copper on the walls of the test tube (right).

On the other hand, the blood-derived carbon could serve as an abundant source of carbon dots through acid treatment of the solid with a H<sub>2</sub>SO<sub>4</sub>-HNO<sub>3</sub> mixture, according to an established protocol [26], except for coal being substituted by our carbon material. In a typical procedure, 300 mg of the blood-derived carbon was suspended in concentrated sulfuric acid (60 mL) and nitric acid (20 mL) followed by sonication for 2 h. The mixture was then

heated under stirring in an oil bath at 120 °C for 24 h. The solution was cooled to room temperature and then neutralized with an aqueous solution of NaOH 3 M in an ice bath. The neutral solution was then dialyzed in 14,000 Da dialysis bag for 5 days against water. A dilute yellowish aqueous solution of carbon dots with an average size of 8 nm was obtained this way (Figure 7).

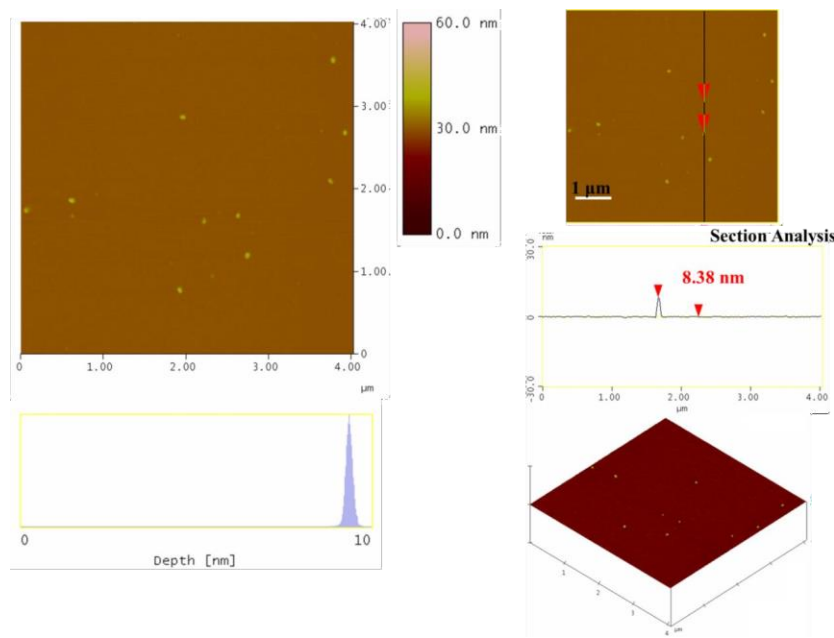


**Figure 7:** Topography images of the as-derived carbon dots (section-analysis, 3D morphology, and depth-analysis histograms are included).

The dots exhibited relatively weak fluorescence (1% quantum yield) mainly in the blue part of the visible region (425 nm), displaying however a small shift up to 450 nm (i.e., still within the blue region) upon excitation between 300-400 nm (Figure 8). This shift could be ascribed to different size sp<sub>2</sub> nanodomains within the dots. In addition, a minor fluorescence peak near 530 nm was also observed, thus signaling the presence of another type of structural fluorophore

to a less extent (e.g., coal-like N-, O- or S-heterocyclic polyaromatics). The position of this peak remained unchanged upon the excitation wavelength. No other emissions were observed in the visible spectrum for higher excitation wavelengths. The weak fluorescence and blue emission of the dots are indicative of high purity carbon dots void of impurities [27].

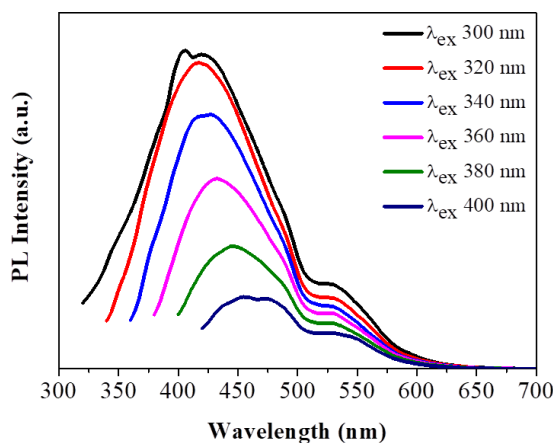


**Figure 8:** Photoluminescence spectra of the as-derived carbon dots in water ( $\lambda_{exc} = 300\text{-}400$  nm).

Lastly, the amorphous carbon nanosheets could be thermally transformed into graphite in two steps: first heat treatment at 1100 oC under an inert Ar atmosphere for 2 h in order to get rid of released gases during heating and then at 1800 oC under vacuum for another 2h. This led to a conductive black powder. XRD showed characteristic peaks attributed to the (002), (101) and (004) reflections of graphite with  $d_{002} = 0.34$  nm [28] (Figure 9, top). In contrast to the parent amorphous carbon nanosheets, no iron-containing phases could be detected in the diffraction pattern probably due to carbon crystallization, which results in more intense diffraction peaks, and the minute amount of iron in the sample. At this point it should be mentioned that heating at higher temperature (e.g., > 2000 oC) is expected to result in even higher degree of

graphitization, nevertheless, we could not reach such high temperatures with our lab ovens. On the other hand, Raman spectroscopy (Figure 9, bottom) showed two strong, sharp bands at 1582 cm<sup>-1</sup> (G: sp<sub>2</sub> carbon) and 1348 cm<sup>-1</sup> (D: sp<sub>3</sub> carbon) with an intensity ratio of ID/IG >1, as well as, weaker bands at 2453 cm<sup>-1</sup> (D + D''), 2681 cm<sup>-1</sup> (2D), 2936 cm<sup>-1</sup> (D + G) and 3228 cm<sup>-1</sup> (2D'). These assignments are well correlated with graphite [21]. Worth noting, the spectrum resembles that of ball-milled graphite bearing structural defects and lattice imperfections due to the impact forces from ball collisions [29]. In our case, such structural defects and lattice imperfections should be aroused from the parent amorphous carbon nanosheets, just like it happens with the graphene oxide-reduced graphene oxide system.

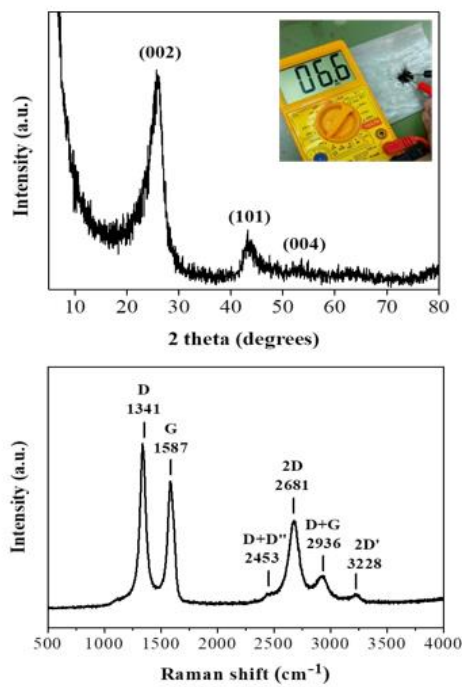


**Figure 9:** XRD pattern (top) and Raman spectrum (bottom) of the derived graphite. The top inset demonstrates the conductive nature of the sample using a 2-point multimeter.

AFM study demonstrated the presence of thick plates with an average thickness of 28 nm (Figure 10), thus

signaling the presence of multilayered graphite.

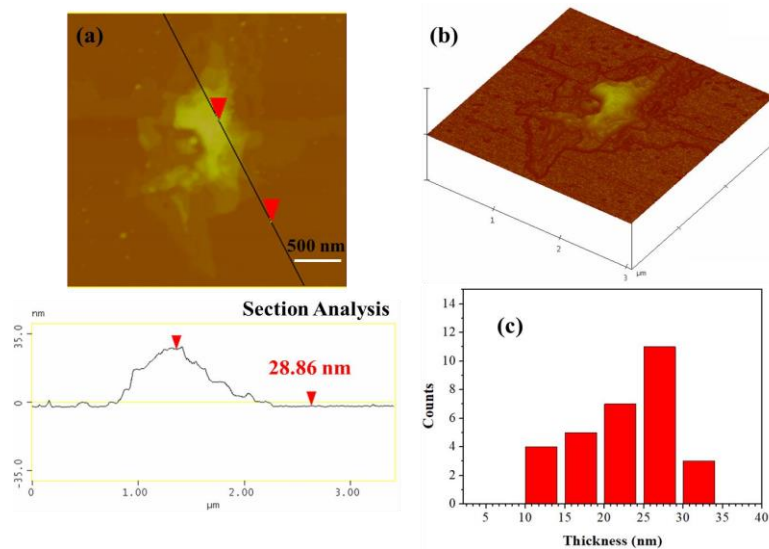


**Figure 10:** (a) AFM image of cross-sectional analysis of a selected graphite plate with an average thickness of 28 nm. (b) AFM image of 3D morphology showing the multilayered texture of the plate, and, (c) statistical analysis of thickness for 30 randomly selected graphitic nanostructures.

The as-prepared graphite could further serve as a source of graphene through the liquid-phase exfoliation technique [30]. To this aim, 25 mg graphite powder was suspended in 5 mL dimethylformamide (DMF) by 2 h sonication in an ultrasound bath using sealed glass vials. The suspension was left for 6 days at ambient conditions

in order to settle down any insoluble particles and the supernatant clear colloid was collected for AFM characterization (Figure 11). Accordingly, graphene layers with an average thickness of 1.5 nm were obtained, i.e., considerably lower than the average thickness of the starting graphite used for exfoliation.

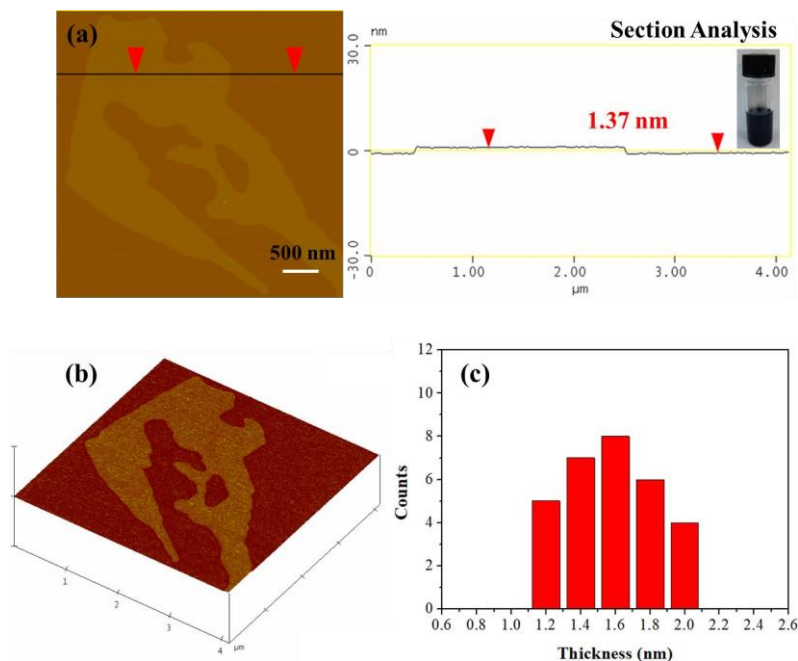


**Figure 11:** AFM cross section analysis profile of a graphene layer. The inset depicts the colloidal dispersion of graphenes in DMF. (b) AFM image of 3D morphology, and, (c) statistical analysis of thickness for 30 randomly selected layers.

### 3.2. Generality of the method

Besides blood, the present microwave approach can be also put forth for medical waste from expired over the counter drugs based on effervescent tablets [31].

As an example here, analgesic paracetamol effervescent tablets (brand name Depon) were directly converted into carbon by microwave heating (Figure 12).



**Figure 12:** Microwave heating of paracetamol effervescent tablets (brand name Depon) resulted in ignition of the tablet and the formation of a carbon residue within the porcelain dish. Washing of the residue with water and acetone afforded a fine carbon powder at yield 25 %.

To this aim, a 500 mg tablet in a porcelain dish was placed in the domestic microwave oven and irradiated at 800 W for 2 min under rotation. This resulted in ignition and carbonization of the tablet

towards the formation of a carbon residue within the dish. Washing of this residue with water and acetone eventually afforded a black powder at yield 25 % (N<sub>2</sub> specific surface area: 200 m<sup>2</sup>/g). The observed

surface area can be attributed to porogen bicarbonate ions present in the effervescent tablet that tend to release CO<sub>2</sub> gas upon heating. Based on XRD and Raman the powder was composed of amorphous carbon (Figure 13), whereas AFM study showed the presence of submicron sized carbon nanosheets with an average thickness of ca. 3.5 nm (Figure 14).

Worth noting, vitamin C or iron and vitamin C effervescent tablets similarly carbonize upon microwave irradiation as above. In fact, in the case of iron a magnetic adduct was obtained due to the reducing power of certain ingredients in the tablet (ascorbic acid, citric acid etc.) [32-34].

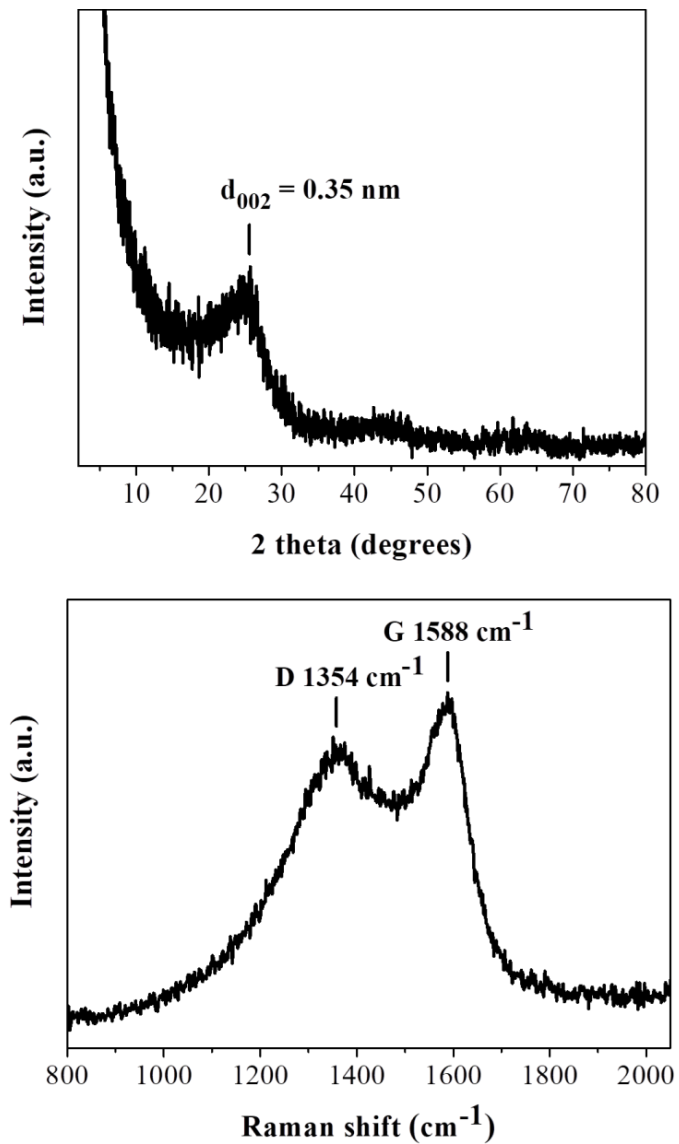


**Figure 13:** XRD pattern (top) and Raman spectrum (bottom) of the tablet-derived carbon.

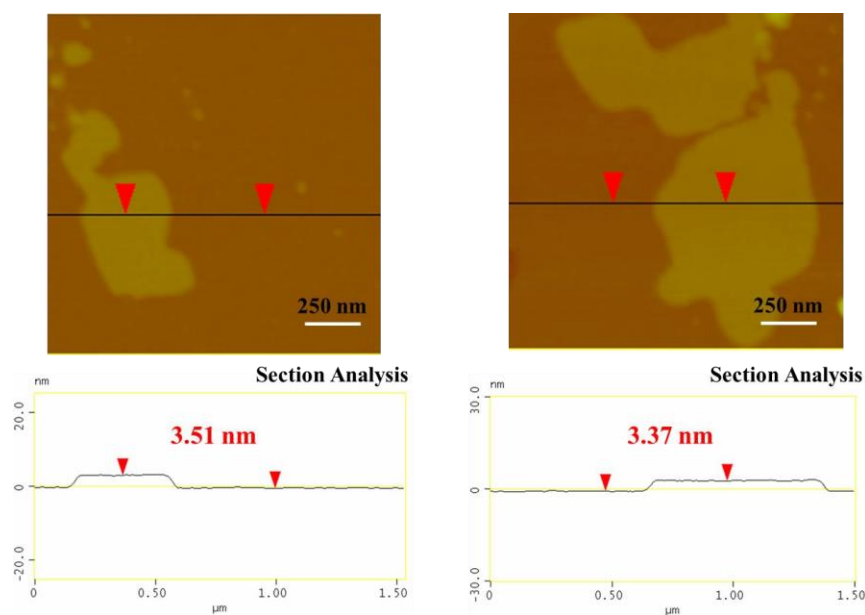


**Figure 14:** AFM images of cross-sectional analysis of selected tablet-derived carbon nanosheets with thickness ca. 3.5 nm.

A practical application of the tablet-derived carbon refers to Cr(VI) removal from wastewaters. Hexavalent chromium Cr(VI) is used in several industrial processes that however produce wastewaters with high levels of this toxic and carcinogenic species [35]. Hence, the removal of Cr(VI) from industrial wastewaters before releasing them into the environment becomes a great necessity. Typically, 18 mg of the carbon material was added to 100 mL aqueous solution of K<sub>2</sub>Cr<sub>2</sub>O<sub>7</sub> in distilled water [concentration of Cr(VI): 6 mg/L] and stirred at room temperature for 24 h in a closed vessel. The pH of the suspension was adjusted to 3 (i.e., the pH of industrial wastewaters) by adding HCl aqueous solution (1 M). During the reaction, at different periods (up to 48 h), 5 mL of the suspension was withdrawn and centrifuged. From the supernatant, 0.3 mL of Cr(VI) solution was used for colorimetric measurements, while the rest was returned to the suspension [36]. The Cr(VI) concentration was determined by the 1,5-diphenylcarbazide method

[37]. Figure 15 shows the effectiveness of the tablet-derived carbon in Cr(VI) removal at initial concentration of 6 mg/L as a function of contact time for pH = 3 at 25 °C. As depicted in the figure, the material shows a fast reaction rate with a Cr(VI) removal efficiency of 40 % within 4 h. However, the reaction rate decreases with increasing reaction time, where the Cr(VI) removal efficiency was calculated at 66 % and 81 % after 24 h and 48 h, respectively. Such removal efficiencies are of particular importance by taking into consideration that the maximum allowed concentration of Cr(VI) in natural waters is 0.1 mg/L while that of drinking water 0.05 mg/L (i.e., half amount). Furthermore, the kinetic data for the material were well interpreted by a second-order model [38]. In fact, the plot of 1/Cr(VI) versus time produced a linear plot (not shown) with correlation coefficient R<sup>2</sup> > 0.99, while the maximum reaction rate for Cr(VI) sorption was estimated at 0.460 mg·L<sup>-1</sup>·h<sup>-1</sup> and the maximum absorption capacity at 25 mg g<sup>-1</sup>.

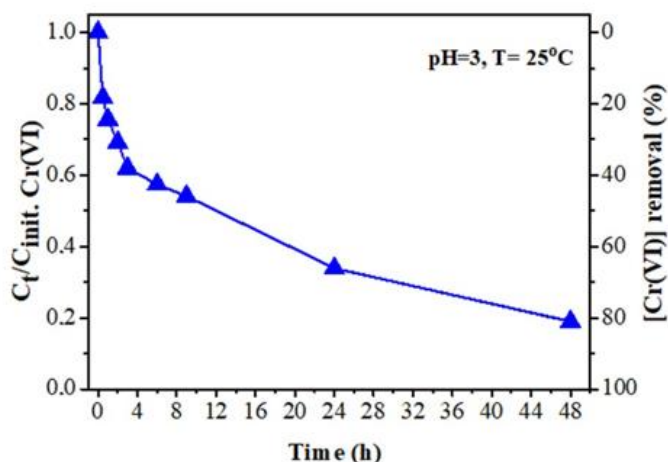


**Figure 15:** Effect of contact time on Cr(VI) removal by the tablet-derived carbon.

#### 4. Conclusions

We have presented the fast and cost-effective microwave synthesis of carbon from bovine blood waste at yield of 2 %. The obtained amorphous solid is composed of large micron-sized nanosheets with an average thickness of ca. 2.5 nm, containing structural O, N and S heteroatoms from blood in the carbonaceous matrix. In addition to these elements, the sample also contained minute traces of the rare iron oxide specularite. In spite the low carbon yield during the microwave and purification steps, the cheap and easy access to large reserves of bovine blood waste from slaughterhouses eventually makes possible the manufacture of a large amount of carbon with well-defined structure and composition from animal blood. This carbon may end up in extractive metallurgy for the carbothermal reduction of ores into metals, as well as, it may serve as feedstock material towards the synthesis of other types of carbon, such as photoluminescent carbon dots, synthetic graphite and graphene. For instance, carbothermal reduction of copper oxide gave copper metal. On the other hand, acidic fragmentation of the blood-derived

carbon according to an established protocol gave water-soluble photoluminescent carbon dots. Lastly, thermal processing of the blood-derived carbon at high temperature gave synthetic graphite, the latter serving as a source of graphene through the liquid-phase exfoliation technique. Apart from blood waste, medical waste pertaining to expired drug effervescent tablets (e.g., analgesic paracetamol) can be also effectively converted under the microwaves into carbon with good Cr(VI) removal efficiency. The present findings show how certain types of waste other than biomass (i.e., animal blood or expired drugs) can be easily converted into valuable carbon materials through simple and friendly microwave technology (e.g., a domestic microwave oven at spot).

#### Conflict of interest

The authors declared that they have no conflicts of interest to this work.

### Acknowledgments

This study was funded by the project “National Infrastructure in Nanotechnology, Advanced Materials and Micro-/Nanoelectronics” (MIS-5002772) which was implemented under the action “Reinforcement of the Research and Innovation Infrastructure”, funded by the Operational Programme “Competitiveness, Entrepreneurship and Innovation” (NSRF 2014-2020), and co-financed by Greece and the European Union (European Regional Development Fund). N. C. gratefully acknowledges the IKY foundation for the financial support. This research was also co-financed by Greece and the European Union (European Social Fund-ESF) through the Operational Programme “Human Resources Development, Education and Lifelong Learning” in the context of the project “Strengthening Human Resources Research Potential via Doctorate Research” (MIS-5000432), implemented by the State Scholarships Foundation (IKY). A. B. acknowledges the funding from the Czech Science Foundation, project GA CR-EXPRO, 19-27454X. V. Š. thanks the Internal Student Grant Agency of Palacký University in Olomouc, Czech Republic (IGA\_PrF\_2021\_031). The authors greatly acknowledge Dr. Ch. Papachristodoulou for the XRD measurements.

### References

- CSF Bah, A El-Din A Bekhit, A Carne, et al. Slaughterhouse blood: an emerging source of bioactive compounds. *Compr. Rev. Food Sci. Food Saf* 12 (2013): 314-331.
- VDM Silva, MPC Silvestre. Functional properties of bovine blood plasma intended for use as a functional ingredient in human food. *LWT-Food Sci. Technol.* 36 (2003): 709-718.
- VM Gorbato. Collection and utilization of blood and blood proteins for edible purposes in the USSR. In: A. M. Pearson, T. R. Dutson, editors. *Edible meat by-products advances in meat research*. London and New York, N. Y.: Elsevier Applied Science (1988): 167-196.
- R Gatnau, J Polo, E Robert. Plasma protein antimicrobial substitution at negligible risk. *Cah. Options Mediterr* 54 (2001): 141-150.
- CZ Guo, CG Chen, ZL Luo. A novel nitrogen-containing electrocatalyst for oxygen reduction reaction from blood protein pyrolysis. *J. Power Sources* 245 (2014): 841-845.
- J Zhang, Q Li, C Zhang, et al. A N-self-doped carbon catalyst derived from pig blood for oxygen reduction with high activity and stability. *Electrochim. Acta* 160 (2015): 139-144.
- J Maruyama, I Abe. Carbonized hemoglobin functioning as a cathode catalyst for polymer electrolyte fuel cells. *Chem. Mater.* 18 (2006): 1303-1311.
- J Maruyama, J Okamura, K Miyazaki, et al. Two-step carbonization as a method of enhancing catalytic properties of hemoglobin at the fuel cell cathode. *J Phys Chem C* 111 (2007): 6597-6600.
- D Chakraborty, S Sarkar, PK Das. Blood Dots: Hemoglobin-derived carbon dots as hydrogen peroxide sensors and pro-drug activators. *ACS Sustain Chem Eng* 6 (2018): 4661-4670.

10. J Li, J Dai, G Liu, et al. Biochar from microwave pyrolysis of biomass: a review. *Biomass Bioenerg.* 94 (2016): 228-244.
11. AM Abioye, FN Ani. Advancement in the production of activated carbon from biomass using microwave heating. *Jurnal Teknologi (Sciences & Engineering)* 79 (2017): 79-88.
12. W Ao, J Fu, X Mao, et al. Microwave assisted preparation of activated carbon from biomass: a review. *Renew. Sustain. Energy Rev.* 92 (2018): 958-979.
13. N Chalmpes, G Asimakopoulos, M Baikousi, et al. Microwave synthesis, characterization and perspectives of wood pencil-derived carbon. *Waste Biomass Valorization* (2021).
14. SB Hladky, MA Barrand. Mechanisms of fluid movement into, through and out of the brain: evaluation of the evidence. *Fluids Barriers CNS* 11 (2014): 26.
15. JA Stokum, V Gerzanich, JM Simard. Molecular pathophysiology of cerebral edema. *J. Cereb. Blood Flow Metab.* 36 (2016): 513-538.
16. N Nakamura, B Reeja-Jayana. Synchrotron X-ray characterization of materials synthesized under microwave irradiation. *J Mater Res* 34 (2019): 194-205.
17. JS Roh. Structural study of the activated carbon fiber using laser Raman spectroscopy. *Carbon Lett.* 9 (2008): 127-130.
18. M Deraman, NES Sazali, MFYM Hanappi, et al. Graphene/semicrystalline-carbon derived from amylose films for supercapacitor application. *J Phys Conf Ser* 739 (2016): 012085.
19. GM da Costa, VG de Resende, NM Toríbio. Quantitative phase analysis of iron ore concentrates. *REM: R. Esc. Minas, Ouro Preto* 55 (2002): 263-266.
20. SH Kim, PB Kelly, AJ Clifford. Biological/biomedical accelerator mass spectrometry targets. 2. Physical, morphological, and structural characteristics. *Anal. Chem.* 80 (2008): 7661-7669.
21. N Chalmpes, K Spyrou, AB Bourlinos, et al. Synthesis of highly crystalline graphite from spontaneous ignition of in situ derived acetylene and chlorine at ambient conditions. *Molecules* 25 (2020): 297.
22. AB Bourlinos, EP Giannelis, Y Sanakis, et al. A graphite oxide-like carbogenic material derived from a molecular precursor. *Carbon* 44 (2006): 1906-1912.
23. S Kundu, Y Wang, W Xia, et al. Thermal stability and reducibility of oxygen-containing functional groups on multiwalled carbon nanotube surfaces: a quantitative high-resolution XPS and TPD/TPR study. *J. Phys. Chem. C* 112 (2008): 16869-16878.
24. H Nishizaka, T Kimura, Y Sato, et al. Slippage-inhibiting effect of interfacial cross-linking of nanotubes by defluorination on the mechanical properties of free-standing multi-walled carbon nanotube yarns: comparison with individual multi-walled carbon nanotubes. *Carbon* 179 (2021): 1-12.
25. D Zaoralova, V Hruba, V Sedajova, et al. Tunable synthesis of nitrogen doped graphene from fluorographene under mild

- conditions. ACS Sustain. Chem. Eng. 8 (2020): 4764-4772.
26. R Ye, C Xiang, J Lin, et al. Coal as an abundant source of graphene quantum dots. Nat. Commun. 4 (2013): 2943.
27. JB Essner, JA Kist, L Polo-Parada, et al. Artifacts and errors associated with the ubiquitous presence of fluorescent impurities in carbon nanodots. Chem. Mater. 30 (2018): 1878-1887.
28. K Jurkiewicz, M Pawlyta, A Burian. Structure of carbon materials explored by local transmission electron microscopy and global powder diffraction probes. C 4 (2018): 68.
29. C Greco, U Cosentino, D Pitea, et al. Role of the carbon defects in the catalytic oxygen reduction by graphite nanoparticles: a spectromagnetic, electrochemical and computational integrated approach. Phys. Chem. Chem. Phys 21 (2019): 6021-6032.
30. AB Bourlinos, V Georgakilas, R Zboril, et al. Liquid-phase exfoliation of graphite towards solubilized graphenes. Small 5 (2009): 1841-1845.
31. M Jaseem, P Kumar, RM John. An overview of waste management in pharmaceutical industry. Pharma Innov. 6 (2017): 158-161.
32. JM May, ZC Qu, S Mendiratta. Role of ascorbic acid in transferrin-independent reduction and uptake of iron by U-937 cells. Biochem. Pharmacol 57 (1999): 1275- 1282.
33. MA Karakassides, D Gournis, AB Bourlinos, et al. Magnetic Fe<sub>2</sub>O<sub>3</sub>-Al<sub>2</sub>O<sub>3</sub> composites prepared by a modified wet impregnation method. J. Mater Chem 13 (2003): 871-876.
34. K Klacanova, P Fodran, P Simon, et al. Formation of Fe(0)-nanoparticles via reduction of Fe(II) compounds by amino acids and their subsequent oxidation to iron oxides. J. Chem 2013 (2013): 961629.
35. M Casadevall, P da Cruz Fresco, A Kortenkamp. Chromium(VI)-mediated DNA damage: oxidative pathways resulting in the formation of DNA breaks and abasic sites. Chem. Biol. Interact. 123 (1999): 117-132.
36. G Asimakopoulos, M Baikousi, V Kostas, et al. Nanoporous activated carbon derived via pyrolysis process of spent coffee: structural characterization. investigation of its use for hexavalent chromium removal. Appl. Sci. 10 (2020): 8812.
37. J Cao, WX Zhang. Stabilization of chromium ore processing residue (COPR) with nanoscale iron particles. J. Hazard. Mater 132 (2006): 213-219.
38. G Asimakopoulos, M Baikousi, C Salmas, et al. Advanced Cr(VI) sorption properties of activated carbon produced via pyrolysis of the “*posidonia oceanica*” seagrass. J Hazard Mater 405 (2021): 124274.



This article is an open access article distributed under the terms and conditions of the [Creative Commons Attribution \(CC-BY\) license 4.0](#)